Electronic Supplementary Information

Construction of 2D heterostructure Fe_2P-CoP_2/MoO_x Nanosheets for Efficient Oxygen Evolution Reaction

Guan Sheng,[a] Yanghang Fang,[b] Shuangyang Zhao,[b] Ruilin Lyu,[a] Huijun Song,*[b] Hui Jin,[b] Hasmaliza Mohamad [a], Che Azurahanim Che Abudullah,[c] Soorathep Kheawhom,[d] Wei Shao,[b] Ruilian Yin,*[b] and Ahmad Azmin Mohamad*[a]

[a] Energy Materials Research Group (EMRG), School of Materials and Mineral Resources Engineering, Universiti Sains Malaysia, 14300 Nibong Tebal, Pulau Pinang, Malaysia

[b] College of Chemical Engineering and State Key Laboratory Breeding Base of Green Chemistry Synthesis Technology, Zhejiang University of Technology, Hangzhou, 310014, China

[c] Department of Physics, Faculty of Science, Universiti Putra Malaysia, 43400 Serdang, Selangor, Malaysia

[d] Department of Chemical Engineering, Faculty of Engineering, Chulalongkorn University, Bangkok 10330, Thailand

Experimental section

Chemical and Materials.

Iron Dichloride ($FeCl_2 \cdot 4H_2O$), Sodium Molybdate Dihydrate ($Na_2MoO_4 \cdot 2H_2O$), Cobalt Nitrate Hexahydrate ($Co(NO_3)_2 \cdot 6H_2O$), Sodium Dihydrogen Phosphate Dihydrate ($NaH_2PO_4 \cdot 2H_2O$), Hydrochloric Acid (HCl), Acetone (CH_3COCH_3), Ethanol (EtOH) and Methanol (MeOH) were acquired as analytical grade.

Synthesis of Ni foam-supported $CoMoO_4$, $FeOOH/CoMoO_4$, Fe_2P-CoP_2/MoO_x, P-$CoMoO_4$, P-FeOOH and NiFe LDH nanosheets.

For the synthesis of NF-supported $CoMoO_4$ nanosheet, 0.175 g $Co(NO_3)_2 \cdot 6H_2O$ (0.6 mmol) and 0.145 g $Na_2MoO_4 \cdot 2H_2O$ were solubilized in 15 mL of DI water. Consequently, the two clear solutions were mixed while being constantly stirred for a duration of 0.5 h, followed by their transfer into a 25 mL autoclave which is Teflon-lined. A portion of pretreated NF was cut into 1 cm× 3 cm and treated using acetone, diluted HCl and ethanol sequentially under sonication for 0.5 h. The pretreated NF was placed in the autoclave described above, and the mixing apparatus was maintained at 150°C for a period of 4 h. Afterward, take out the NF sample, clean, and vacuum dry to obtain NF-supported $CoMoO_4$.

For the synthesis of $FeOOH/CoMoO_4$ nanosheet, $FeCl_2 \cdot 4H_2O$ (100 mg) was dissolved in a mixed solution of 4 ml DI water and 16 ml ethanol using ultrasound for 3 min and then moved into a 25 ml Teflon-lined autoclave. Afterward, the as-synthesized $CoMoO_4$ nanosheet was vertically put into a Teflon autoclave and reacted for 12 h at 90°C. After reaching the temperature of room, the $FeOOH/CoMoO_4$ nanosheet was washed many times with DI water and ethanol and dried under 60°C overnight.

For the synthesis of Fe_2P-CoP_2/MoO_x nanosheets, the as-prepared $FeOOH/CoMoO_4$ and 0.5 g $NaH_2PO_4 \cdot 2H_2O$ were put at the downstream and upstream sides of the tubular furnace. Before phosphatization, N_2 was purged for 30 min to remove air. Subsequently, the tubular furnace was set to 350°C with a heating ramp of 2°C min^{-1} for 2 h under flowing N_2 to achieve the final product. For comparison, phosphated $CoMoO_4$ (P-$CoMoO_4$) nanosheets and phosphated FeOOH (P- FeOOH) nanosheets are under the same process.

For the synthesis of NiFe LDH, dissolve 0.5 mmol $Ni(NO_3)_2$ $6H_2O$, 0.5 mmol $Fe(NO_3)_3$ $9H_2O$ and 4 mmol $CO(NH_2)_2$ in 35 ml of DI water in a Teflon-lined stainless-steel autoclave. Correspondingly, a piece of NF pretreated with acetone and hydrochloric acid is put into it. Seal the autoclave and keep it at 120℃ for 12 h. After

the autoclave is cooled to room temperature, remove the reactive NF, rinse with a large amount of water and ethanol, and vacuum dry overnight.

Materials characterizations.

Utilizing a ZEISS-G500 FESEM, images were captured at an accelerating voltage of 5 kV. The samples obtained from the NF were subjected to analysis using an FEI Talos Transmission Electron Microscope (TEM) for the acquisition of TEM images, EDS spectrum and elemental mapping. ACTEM images were captured using an FEI Titan Transmission Electron Microscope (TEM) which is equipped with a spherical aberration corrector integrated into the objective lens. Additionally, X-ray Diffraction (XRD) was performed using a D8 Advance instrument (Bruker) with Cu Kα radiation for the determination of crystalline phase characteristics. All samples' surfaces properties were assessed utilizing ESCALAB 250 X-ray Photoelectron Spectroscopy equipment (XPS), calibration of binding energies was obtained using the C 1s peak at 284.8 eV.

Electrochemical measurement.

Electrochemical performance was evaluated in 1.0 M Potassium hydroxide (KOH) with a standard three-electrode system via an CHI 760E electrochemical workstation, which was the NF-supported catalysts (WE), the saturated Ag/AgCl electrode (RE) and Pt (CE). Consequently, the measured potentials were adjusted to a RHE using the formula of $E_{RHE} = E_{Ag/AgCl} + 0.059 \times pH + 0.197$ (V). LSV curves for OER adjusted employing 90% iR compensation. On the other hand, the electric double-layer capacitance was measured at different scan rates in the non-Faraday potential range.

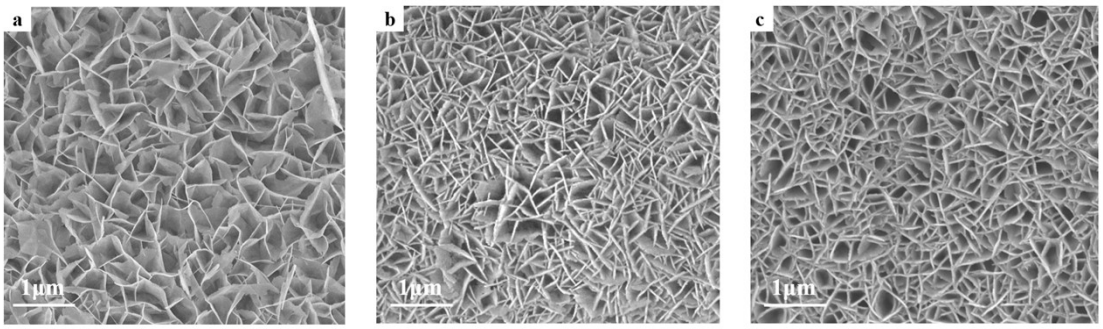

Figure S1. Low -magnification SEM images of (a-c) $CoMoO_4$, $CoMoO_4$-FeOOH and Fe_2P-CoP_2/MoO_x nanosheets

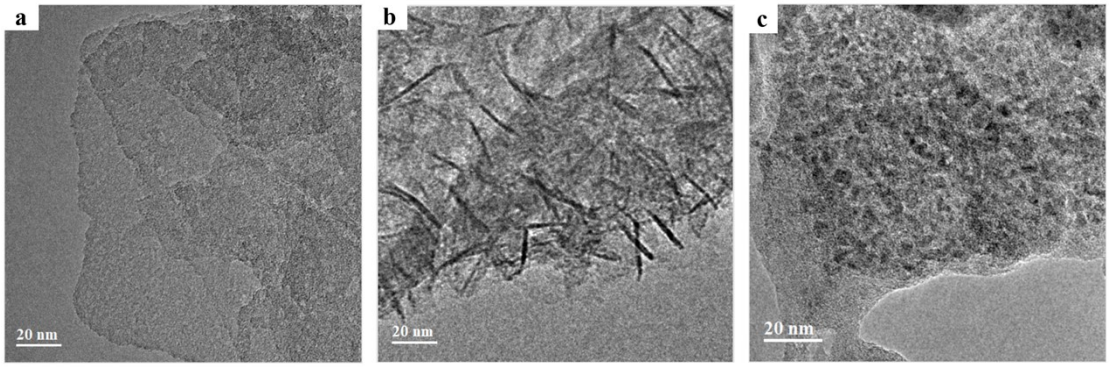

Figure S2. Low-magnification TEM images of (a-c) $CoMoO_4$, $CoMoO_4$-FeOOH and Fe_2P-CoP_2/MoO_x nanosheets

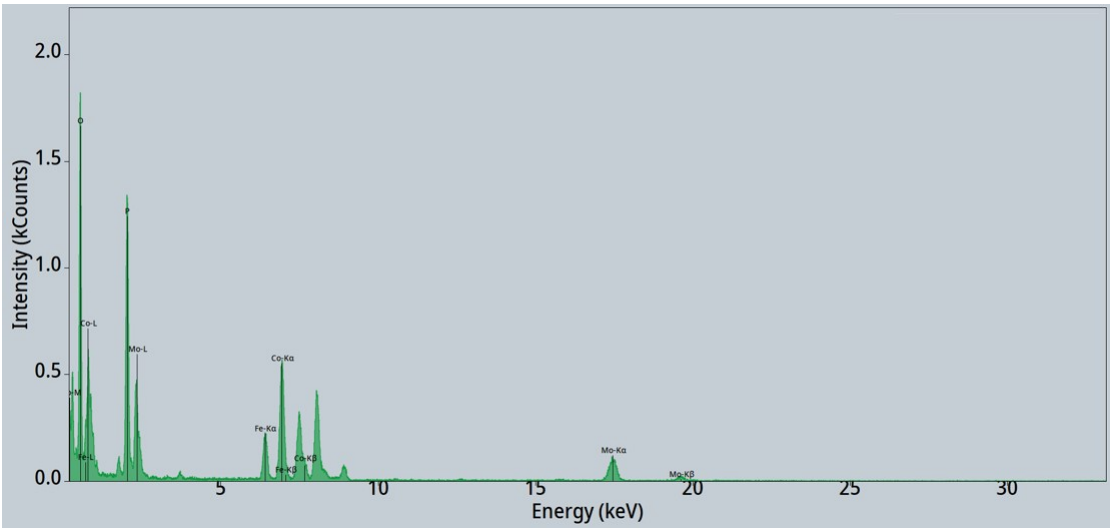

Figure S3. EDS spectrum of Fe_2P-CoP_2/MoO_x nanosheets.

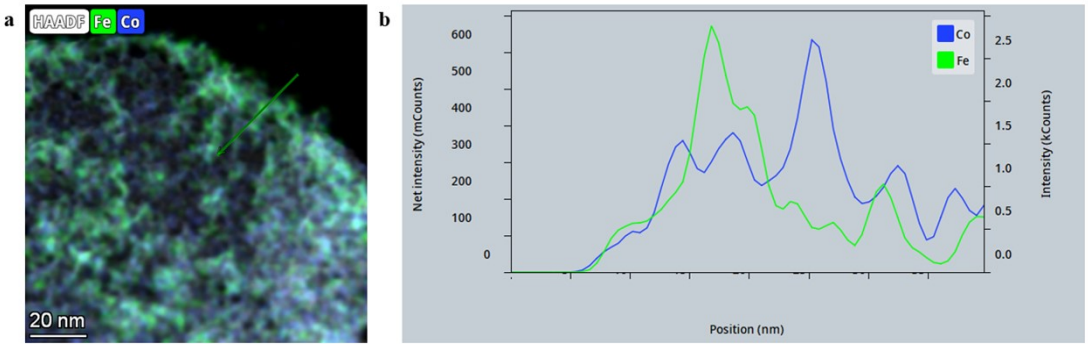

Figure S4. (a)Merged image for HAADF STEM, Fe and Co EDS mapping images of Fe_2P-CoP_2/MoO_x nanosheets. (b) EDS Line scan spectrum of the area marked with green arrow in (a)

Table S1. Atomic fraction and mass fraction of O, P, Fe, Co, Mo elements from EDS spectrum of Fe_2P-CoP_2/MoO_x nanosheets.

Z	Element	Family	Atomic Fraction (%)	Atomic Error (%)	Mass Fraction (%)	Mass Error (%)	Fit error (%)
8	O	K	48.78	5.18	21.44	1.47	2.61
15	P	K	22.38	4.84	19.04	3.82	1.25
26	Fe	K	4.42	0.74	6.79	1.00	0.37
27	Co	K	11.44	1.93	18.52	2.73	0.87
42	Mo	K	12.98	2.15	34.20	4.95	0.30

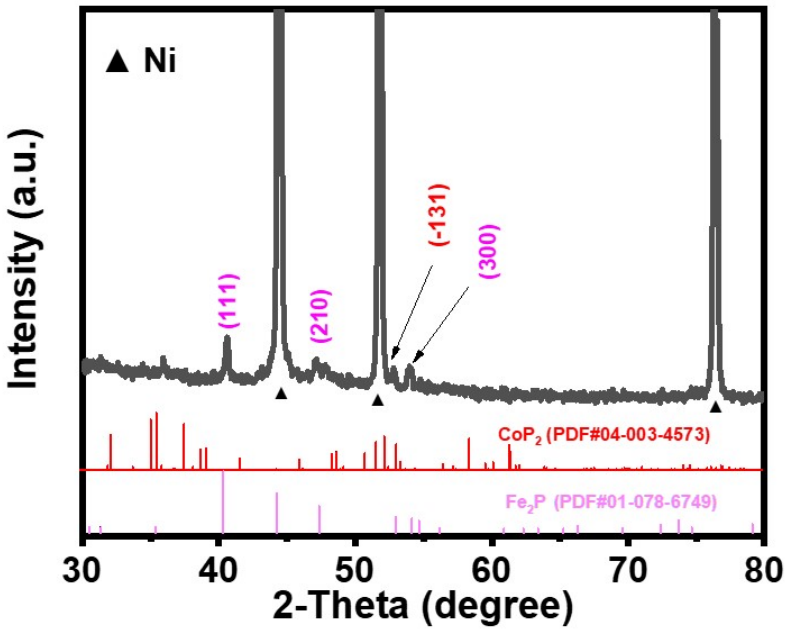

Figure S5. XRD patterns of Fe_2P-CoP_2/MoO_x nanosheets.

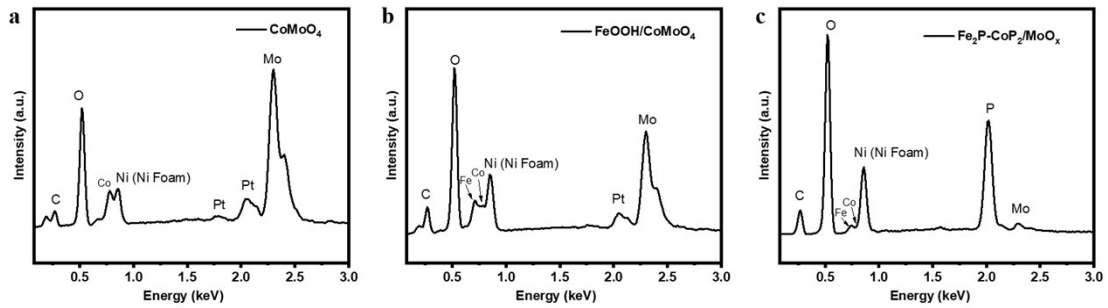

Figure S6. SEM EDS spectrum of (a) $CoMoO_4$, (b) $FeOOH/CoMoO_4$ and (c) Fe_2P-CoP_2/MoO_x nanosheets.

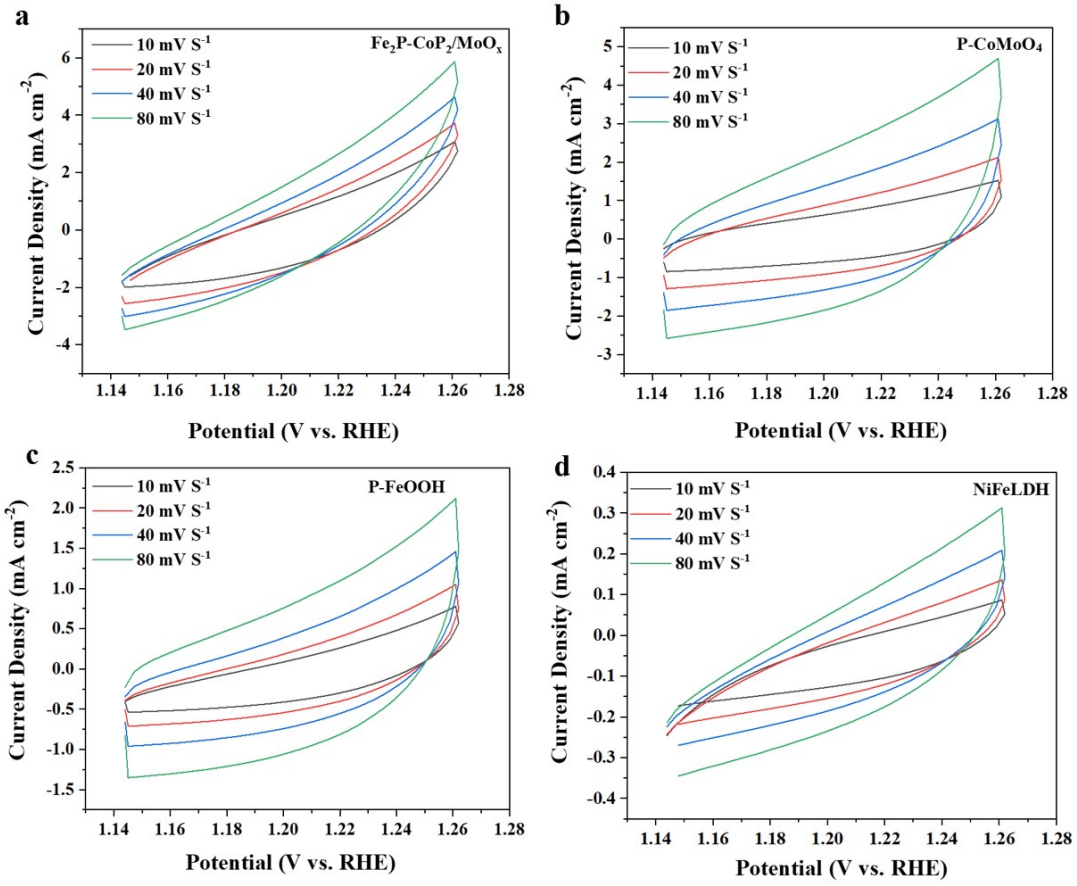

Figure S7. CV curves of (a) Fe_2P-CoP_2/MoO_x, (b) P-$CoMoO_4$, (c) P-FeOOH and (d) NiFeLDH at the different scan rates from 10-80 mV s^{-1}.

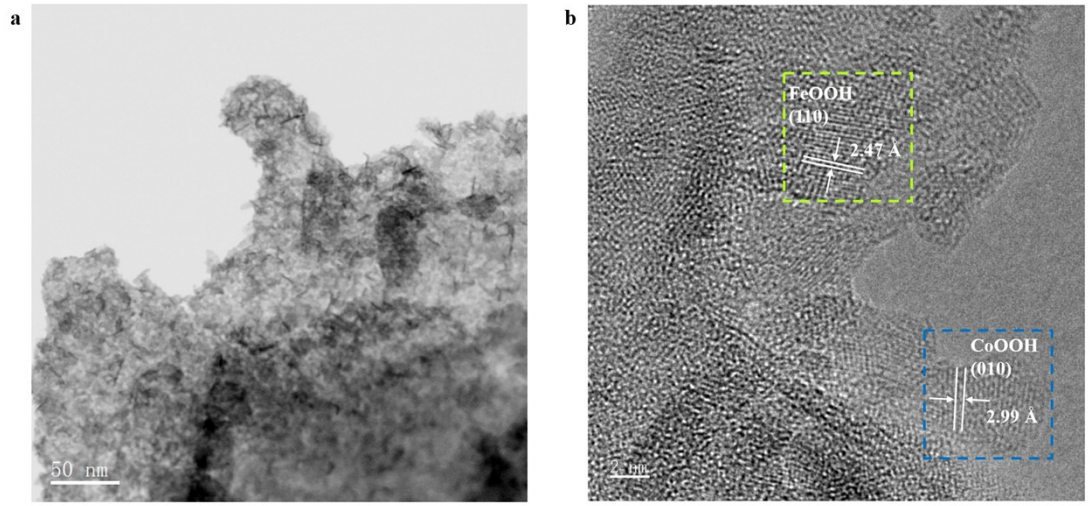

Figure S8 Low-magnification and high-resolution TEM images of Fe_2P-CoP_2/MoO_x after LSV test.

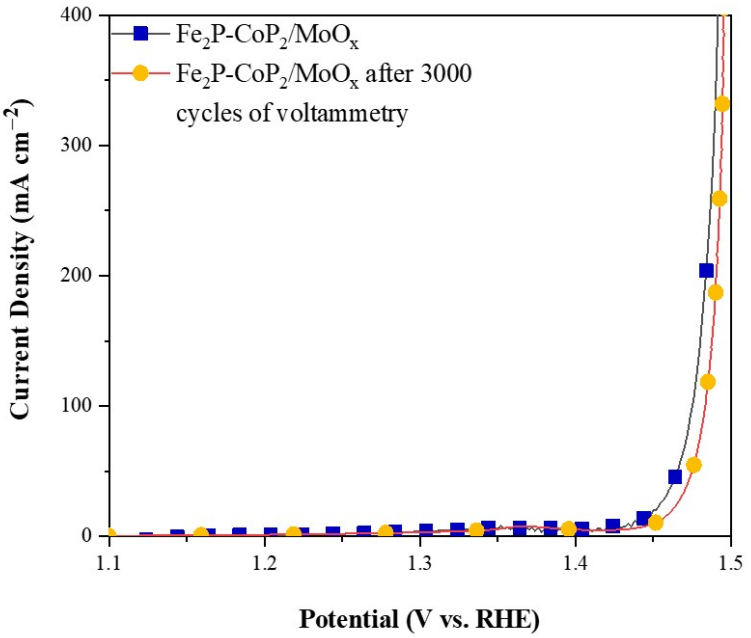

Figure S9 The OER performance of the as-prepared catalyst; polarization curves for Fe_2P-CoP_2/MoO_x, Fe_2P-CoP_2/MoO_x after 3000 cycles of voltammetry

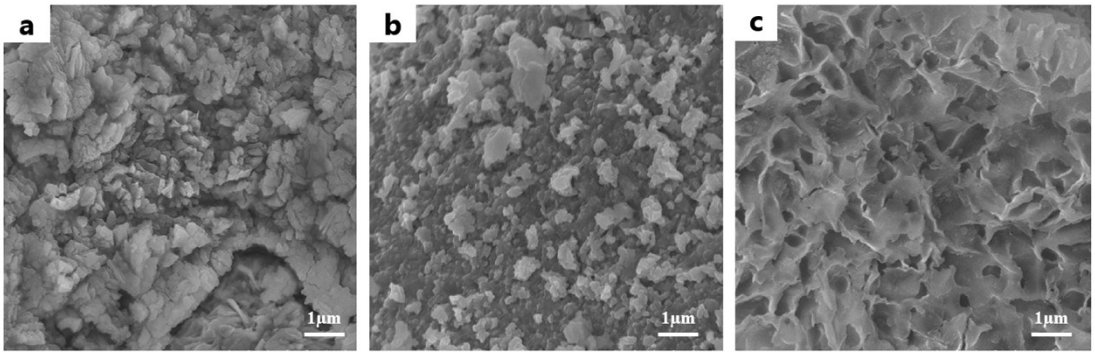

Figure S10 SEM images of (a) P-$CoMoO_4$, (b) P-FeOOH and (c) Fe_2P-CoP_2/MoO_x after LSV test.

Table S2. Comparison of OER performances between Fe_2P-CoP_2/MoO_x electrode and recently reported electrocatalysts in alkaline solution.

Catalyst	Substrate	Overpotential (mV)	Tafel slope (mV dec^{-1})	Stability	Ref.
Fe_2P-CoP_2/MoO_x	[a]NF	204, 235, 245 @10, 50, 100 mA cm^{-2}	33.3	40 h@50mA cm^{-2}	**This work**
APPJ-Ni_xO_y	NF	355@10 mA cm^{-2}	88	10 h@10 mA cm^{-2}	1
CoO@FeBTC	NF	255@100 mA cm^{-2}	40	100 h@500 mA cm^{-2}	2
Fe_3S_4	NF	251@10 mA cm^{-2}	45.9	12 h@18 mA cm^{-2}	3
NiCo-P	NF	315,378,416@100, 500,1000 mA cm^{-2}	66	30 h@100,500, 1000mA cm^{-2}	4
Co_9S_8@$CoNi_2S_4$	NF	170@10 mA cm^{-2}	56	24 h@10 mA cm^{-2}	5
P-CoFe-LDH@MXene	NF	252@200 mA cm^{-2}	98.59	100 h@10 mA cm^{-2}	6
$NiCoFeO_xH_y/Ni_3S_2$	NF	254@100 mA cm^{-2}	30.1	9 h@20 mA cm^{-2}	7
NiS_2-MoS_2	NF	210@10 mA cm^{-2}	58	48 h@10 mA cm^{-2}	8
FeCoNiP	NF	281,318@500, 1000 mA cm^{-2}	35	48 h@500 mA cm^{-2}	9
$FeCo_2Mo_5$ LDH/Ni_3S_2	NF	128, 300@10, 100 mA cm^{-2}	72.5	12 h@95 mA cm^{-2}	10
FeNiP NSs	[b]CC	233@10 mA cm^{-2}	45.2	40 h@10, 100 mA cm^{-2}	11
CoP/FeP_4	[c] CNT	301@10 mA cm^{-2}	48	20 h@10 mA cm^{-2}	12
Co_9S_8-ZnS	[d]NTC	290@10 mA cm^{-2}	69	40000 s@10 mA cm^{-2}	13

[a] NF; nickel foam, [b] CC; carbon cloth, [c] CNT; carbon nanotubes, [d] NTC; carbonaceous nanotube.

References

1. B. Zhang, X. Shang, Z. Jiang, C. Song, T. Maiyalagan and Z. J. Jiang, *ACS Applied Energy Materials*, 2021, **4**, 5059-5069.
2. Y. W. Dong, F. L. Wang, Y. Wu, X. J. Zhai, N. Xu, X. Y. Zhang, R. Q. Lv, Y. M. Chai and B. Dong, *Journal of Colloid and Interface Science*, 2023, **645**, 410-419.
3. A. Kundu, B. Kumar and B. Chakraborty, *Journal of Physical Chemistry C*, 2022, **126**, 16172-16186.
4. Z. Xu, C.-L. Yeh, J.-L. Chen, J. T. Lin, K.-C. Ho and R. Y.-Y. Lin, *ACS Sustainable Chemistry & Engineering*, 2022, **10**, 11577-11586.
5. W. Chen, Y. Hu, P. Peng, J. Cui, J. Wang, W. Wei, Y. Zhang, K. K. Ostrikov and S. Q. Zang, *Science China Materials*, 2022, **65**, 2421-2432.
6. L. Deng, K. Zhang, D. Shi, S. Liu, D. Xu, Y. Shao, J. Shen, Y. Wu and X. Hao, *Applied Catalysis B: Environmental*, 2021, **299**, 120660.
7. Y. Fan, W. Shi and L. Li, *Inorganic Chemistry*, 2023, **62**, 1561-1569.
8. W. Xu, Y. Wei, S. Zhou, R. Sun, X. Huang, S. Han, S. Wang and J. Jiang, *Electrochimica Acta*, 2023, **454**.
9. R. Liu, T. Song, H. Xue, J. Sun, N. Guo, J. Sun, Y. R. Hao and Q. Wang, *ACS Applied Energy Materials*, 2023, **6**, 692-701.
10. Y. Huang, J. Peng, Y. Gao, Z. Wang, J. Li and F. Li, *ACS Applied Energy Materials*, 2022, **5**, 12937-12944.
11. Y. Liu, F. Luo, X. Jiang, B. Yuan and S. Chen, *International Journal of Hydrogen Energy*, 2022.
12. Y. Liu, Y. Li, Q. Wu, Z. Su, B. Wang, Y. Chen and S. Wang, *Nanomaterials*, 2021, **11**, 1450.
13. Y. Yang, D. Wang, Y. Wang, Z. Li, R. Su, X. Wang, T. Xu and S. Wang, *ACS Applied Energy Materials*, 2022, **5**, 14869-14880.